2020 IEEE/RSJ International Conference on Intelligent Robots and Systems (IROS)
October 25-29, 2020, Las Vegas, NV, USA (Virtual)

Soft Microrobotic Transmissions Enable Rapid Ground-Based Locomotion

Wei Zhou and Nick Gravish *Member, IEEE*

***Abstract*— In this paper we present the design, fabrication, testing, and control of a 0.4 g milliscale robot employing a soft polymer flexure transmission for rapid ground movement. The robot was constructed through a combination of two methods: smart-composite-manufacturing (SCM) process to fabricate the actuators and robot chassis, and silicone elastomer molding and casting to fabricate a soft flexure transmission. We actuate the flexure transmission using two customized piezoelectric (PZT) actuators that attach to the transmission inputs. Through high-frequency oscillations, the actuators are capable of exciting vibrational resonance modes of the transmission which result in motion amplification on the transmission output. Directional spines on the transmission output generate traction force with the ground and drive the robot forward. By varying the excitation frequency of the soft transmission we can control locomotion speed, and when the transmission is oscillated at its resonance frequency we achieve high speeds with a peak speed of 439 mm/s (22 body lengths/s). By exciting traveling waves through the soft transmission, we were able to control the steering direction. Overall this paper demonstrates the feasibility of generating resonance behavior in millimeter scale soft robotic structures to achieve high-speed controllable locomotion.**

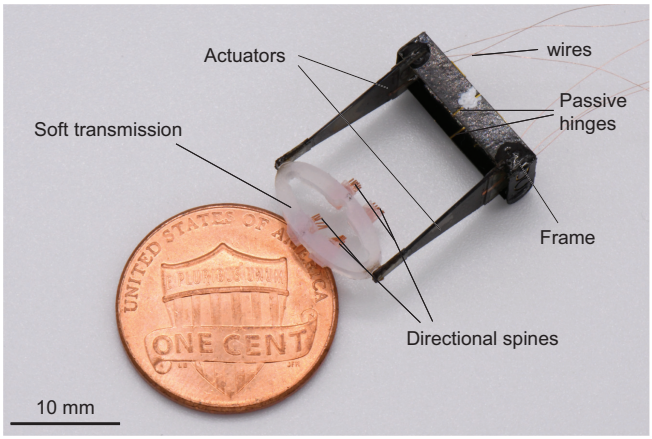

Fig. 1. Millirobot with soft transmission. Two piezoelectric actuators are connected at their base to a rigid carbon-fiber chassis. Passive hinges along the mid-line of the chassis allow the robot to flex. The tips of the actuators are connected to a silicone soft robotic transmission. Pairs of directional spines are attached to the output of the transmission.

I. INTRODUCTION

Millimeter scale robots (millirobots) have potential applications in the near future for autonomous navigation and inspection in hard to reach environments [1]. Millirobots can fit within narrow channels and confined spaces such as pipes, between walls, and within the crevasses of rubble. Furthermore, millirobots also have the potential for large quantity production and thus could be fabricated and deployed rapidly at the site of use [2].

Motivated by these applications, researchers have built numerous milliscale robots in prior work [3], [4], [5], [6], [7], [8], [9]. As the scale of robots decreases such that components or even the whole robot are one to several millimeters, standard parts, such as bolts-and-nuts, gears, and rotary elements such as bearing, are no longer commercially available or feasible for design. Novel methods have been developed to build robots at small scales over the years. 3D printing technology has been used to build small-scale robots from the 6 g 3DFlex robot [10] to a 1 mg legged microrobot [11]. The smart-composite-method [12], [13] has been used to build a 1.7 g hexapod HAMR^3 [5], a 3 cm flapping-wing MAV [14], and many more examples. Similar origami approaches that utilize substantial material folding [15], [16] have also been developed for miniature robots. Advances in smart materials have also enabled development of millimeter scale soft-bodied robots [17].

Different ground locomotion methods have been adopted by millirobots in previous work to adapt to various environments. Wheeled locomotion [3] is fast and efficient, however, friction at the rotational joint becomes problematic as the dimension of a robot decreases. Legged robots [4], [5] with multiple degree of freedom (DOF) limbs possess the advantage of traversing rough terrain, while it also adds complexity to the robot fabrication. Vibration driven bristlebots [18], [19], [20] generate forward movement through angled spines. Crawling motion inspired by caterpillar terrestrial locomotion is also used in ground robots [6], which can be modeled as a two-anchor system in which two contact points successively push, and then pull the body forward in a repeating pattern. Our robot utilized this push-pull motion to propel itself forward.

Robots fabricated by rigid materials can provide precise and predictable motion. However, the link-joint structure of rigid robots, even at the millimeter scale, can limit or even inhibit novel dynamics that may be useful for locomotion purposes. Furthermore, generating complex articulated motion with rigid robots requires multiple actuated DOF, which can be an extreme challenge in micro robots with limited power and actuation capabilities. Lastly, microrobots with their ability to explore confined spaces may further benefit from adopting soft robotic components to enable abilities such as squeezing, stretching, growing, and morphing [21].

W. Zhou and N. Gravish are with the Department of Mechanical & Aerospace Engineering, University of California at San Diego, CA, 92093 USA. Contact e-mail: ngravish@ucsd.edu

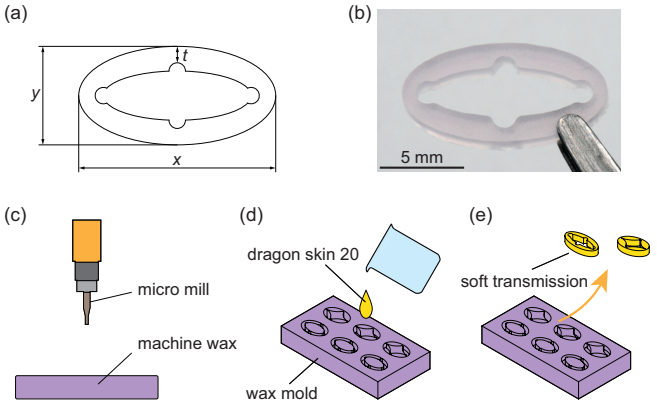

Fig. 2. Soft transmission design and fabrication. (a) Transmission dimensions. (b) Silicon rubber soft transmission. (c) Building mold using micro mill. (d) Casting with *Dragon Skin 20*. (e) Remove parts from mold.

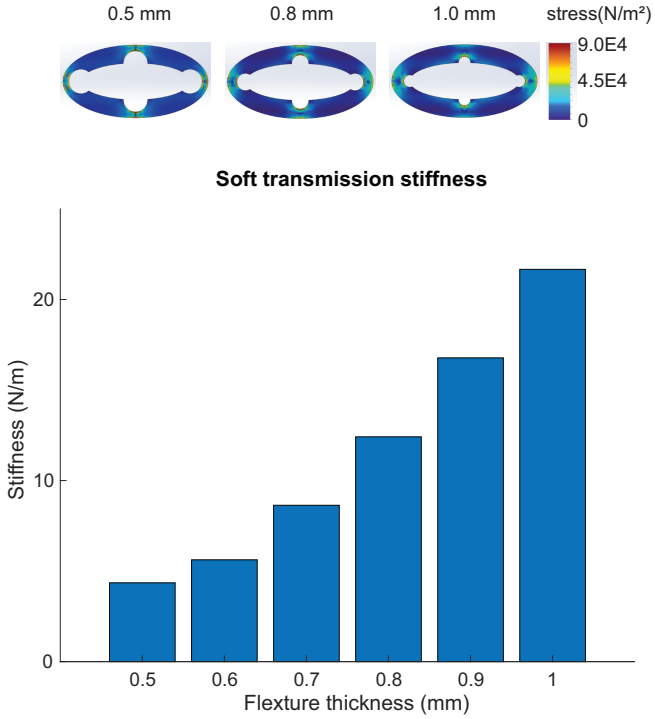

Fig. 3. Finite-element-analysis of the soft transmission results in an increasing stiffness with increasing wall thickness. Above plot shows snapshots of stress during typical deformation.

As an initial step towards bringing soft robotics components to millirobots we seek to develop and study the locomotion capabilities of a vibrationally actuated soft transmission. Many examples of soft robots and soft robotic components are fabricated from flexible, elastic polymers such as silicone rubber. Silicone is an easily castable polymer that is capable of large extension, is highly elastic, and is extremely resilient to a variety of adverse environmental conditions. For the purposes of locomotion the elastic properties of a soft robotic transmission may enable optimal vibrational behaviors such as resonance for rapid locomotion. Furthermore, a soft robotic transmission would be capable of a continuum of deformations, and thus actuation could be programmed to generate complex vibrational wave forms through the transmission to enable robot steering.

In this manuscript we explore the capabilities of using a soft robotic transmission for generation of high-speed ground locomotion. We describe the design, fabrication, testing, and steering control of a milliscale robot 20 mm in body length, that uses two pairs of spines attached to an ellipse-shaped compliant soft robotic transmission. We present design parameters for the soft transmission and measure its dynamic properties in experiments. Open-loop locomotion experiments display fast relative speed capabilities of up to 22 body lengths/s. Steering control is achieved by PZT actuator phase modulation.

II. Soft Transmission Design

PZT actuators have been widely used in micro robots because of their high power density, fast response, steady performance, and high bandwidth [22], [23]. However, due to the stiff materials they are composed of most PZT actuators have a limited deflection range and to achieve larger deflection is often at the sacrifice of force output. Thus, integration of PZT actuators into milliscale robots has spawned the development of novel displacement amplifying mechanisms.

A. Ellipse shape soft transmission

We chose an elliptical shaped soft robotic flexure as our base shape for our millirobot transmission. The aspect ratio of the ellipse was chosen such that small amplitude deflection inputs on the lateral sides of the transmission result in larger output deflections. We integrated variable size cutouts into the ellipse transmission at the lateral and vertical quadrants. These cutouts enabled more focused displacements at these regions and the control of the wall thickness, t, at these cutouts enabled transmission stiffness control, Fig. 2a. Based on previous work of modeling flexure-based mechanism [24], [25], the transmission dimensions of $x = 12$ mm, $y = 6$ mm can provide an amplifying ratio of approximately $n = 2$, as shown in Fig. 2a. Although displacement amplification can result in a decrease of output force, our PZT actuators can still provide sufficient driving force to the robot. A variety of shapes of soft transmissions (for example diamond shaped, bridge shaped, as shown in Fig. 2e) were tested which turned out to be equivalent to the elliptical shaped ones with different wall thickness, t. Thus we focused on analyzing the influence of wall thickness on dynamic properties of the soft transmissions. However, an opportunity we seek to explore in this soft transmission is how deviations from link-flexure based rigid transmissions can be exploited for locomotion capabilities.

B. Soft transmission molding and casting

To fabricate the soft transmission we needed to be able to precisely generate negative molds for them. The size of the transmissions prohibit 3D printing and instead we found machining with a desktop mill to be an economical option. We fabricated molds from machine wax using a commercial micro mill (Othermill). We used an end mill of size $1/64$

inch in diameter which enabled us to build soft transmissions with flexure thickness t ranging from 0.5 mm to 1.0 mm. The machining process took approximately one hour and we generated five molds for each transmission shape profile.

We used a commercially available silicone polymer, Dragon Skin 20, to cast the transmissions. We mixed Dragon Skin 20 part A and part B at ratio 1 : 1 for 10 minutes and then poured into the mold. The silicone rubber was set to rest and cure at room temperature for 4 hours. We manually removed the transmissions after curing completion Fig. 2b. After removal from the mold transmissions were ready to be integrated into the robot.

C. Soft transmission static stiffness

We used a finite element method (FEM) analysis to analyze the static stiffness of the silicone rubber soft transmissions. We developed a 3D model of the transmission in SolidWorks and then used built-in FEM analysis to generate a prediction of stiffness change with transmission geometry. We observed that stress concentrations occurred at the cutouts of the soft flexure, where its thickness is small, as would be expected. For the the thin walled transmission (0.5 mm), the cutouts enabled the transmission to act somewhat like a series of four revolute joints and links at the thin flexure. However, the larger thickness walls behaved more like a continuum elastic structure with more homogeneous stress and strain distribution throughout the transmission. The continuum motion of the transmission body enables shape control and contributes to steering capabilities that wouldn't be possible with a rigid joint-link transmission.

D. Soft transmission dynamic proprieties

As a first determination of the the applicability of a soft transmission for ground locomotion we measured the resonant oscillations of each transmission design. Experiments were conducted to test the dynamic proprieties of a series of soft transmission with different flexure thicknesses. We mounted each transmission between two symmetric bimorph PZT actuators with a fixed base. The actuators were driven by a sinusoidal voltage signal from 10 Hz to 260 Hz to test the dynamic response of the soft transmission system and find out the optimal operating frequency. Experiments with individual actuators have resolved their resonant frequency to be above 1 kHz when not attached to a load. A high-speed camera was set up with a variable frame rate equal to 20 times the driving signal frequency to capture the vibrational motion of the soft transmissions as shown in Fig. 4a. We then tracked the input motion Δx of the two PZT actuators and the output motion Δy of the soft transmissions by analyzing videos in MATLAB, as shown in Fig. 4b. Δx and Δy are the change of distance of two actuating tips and two output tips. The ratio of output amplitude to input amplitude reflects the transmission ratio of the amplitude.

We built 3 batches of each soft transmission design with different flexure thicknesses and tested their dynamic properties individually. Figure 4c shows the frequency response of all soft transmissions with each trial overlaid. The dynamic

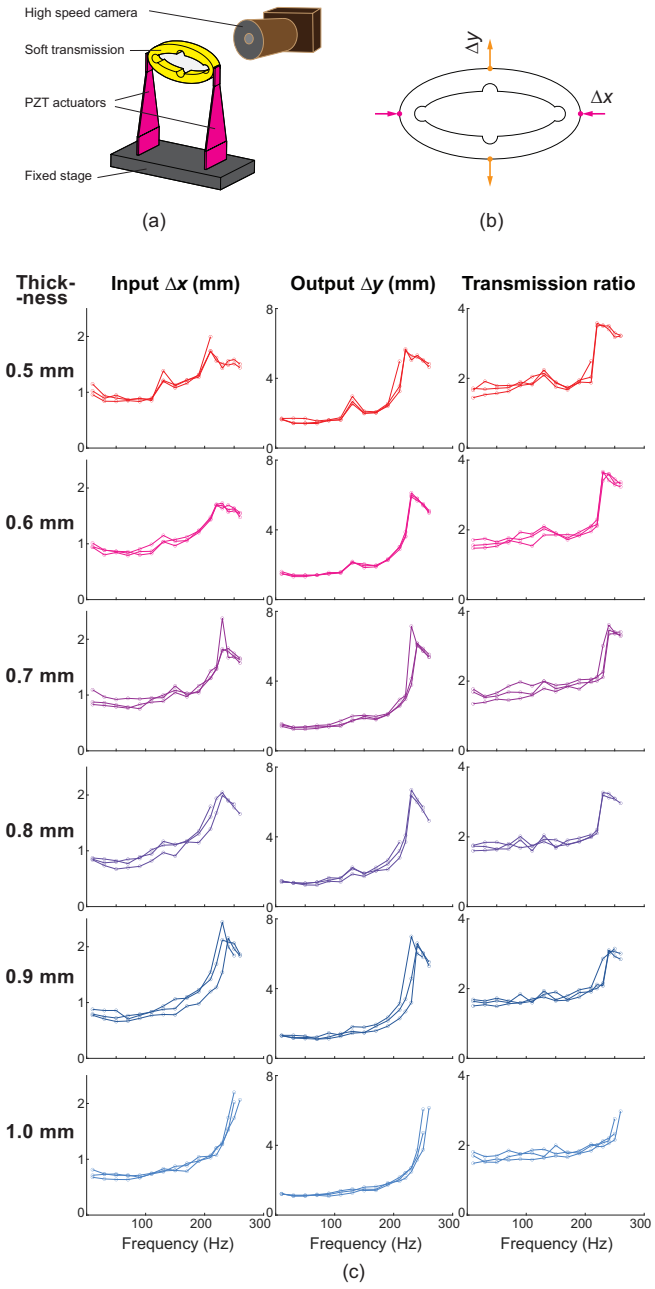

Fig. 4. Dynamic properties of soft transmission. (a) Experiment setup. (b) Tracking input Δx and output Δy. (c) Frequency response of soft transmissions with different flexure thickness.

behavior of soft transmissions from different batches have quite consistent performances. The standard deviation of the soft transmission input and output are 0.06 mm and 0.15 mm respectively. It suggests that wide-scale production of milliscale soft robot components may be achieved through this process. The silicone rubber soft transmissions act as mass-spring systems, and we observe that all transmission-actuator combinations exhibit a resonance mode between 200 Hz to 260 Hz depending on their flexure thickness. Predictions of the resonance frequency is complicated by the stiffness of the actuators (which are in series with the transmission), and the varying transmission mass with varied

geometry. However, general trends may be observed such as the smaller flexure thicknesses result in soft transmissions with lower effective stiffness, and a lower resonance frequency. The transmission ratios at low driving frequency are approximately 2, which matches the prediction from our transmission design. However, the ratios have a significant jump at the system resonance frequency because the input and output amplitudes are larger and the working range of transmissions has shifted. The large amplitude oscillations at resonance are an ideal actuation target to potentially achieve high-speed ground based movement.

III. Robot Design

A. Robot Fabrication

The chassis of the robot is fabricated through the smart-composite-manufacturing (SCM) process. The SCM process consists of laser cutting layers of structural, flexural, and adhesive sheets, and then bonding them together. A final release cut removes the articulated component with joints and links from the supporting scaffold. Furthermore, this same process can be used to cut and fabricate piezoelectric actuators. Carbon fiber layers were used to build the structure of the frame, while two passive Kapton hinges were created on the robot frame along the central axis to couple the flexible bending of the soft transmission.

Two bimorph PZT actuators were used for actuation on our robot. The actuators are 15 mm in total length, where the PZT plate is an isosceles trapezoid whose height is 10 mm and two bases are 1.5 mm and 6 mm respectively. The two PZT actuators were assembled symmetrically across the central axis of a carbon fiber SCM fabricated frame. The actuators were rigidly attached to the frame with epoxy, and power wires were soldered to the base of the actuators. The soft transmission with wall thickness, $t = 0.8$ mm, was attached to the actuator tips using super glue carefully applied to the transmission edges. To enable ground traction, we attached directional spines to the output of the transmission. The directional spines were made by an array of copper wires of diameter 0.1 mm whose front ends were sealed in silicon rubber while rear ends were bent to 45° with respect to ground. The dimension of the robot is 15 mm × 20 mm and the weight is 0.4 g. The robot with a reference object is presented in Fig.1.

B. Robot locomotion

We conducted experiments to investigate the robot locomotion performance on sandpaper of 1 micron grid size. The robot was driven by two PZT actuators at frequency from 10 Hz to 250 Hz, while its locomotion was captured by a high speed camera from above, as shown is Fig. 5a.

For open-loop trials the two actuators were provided with two identical sinusoidal signals at same amplitude and 0° phase difference. The robot trajectories of locomotion in the $x-y$ plane were recorded and shown in Fig. 5b. With no amplitude or phase difference of the actuator control signals, the robot trajectories in the lateral direction demonstrate a random pattern which was caused by the initial conditions

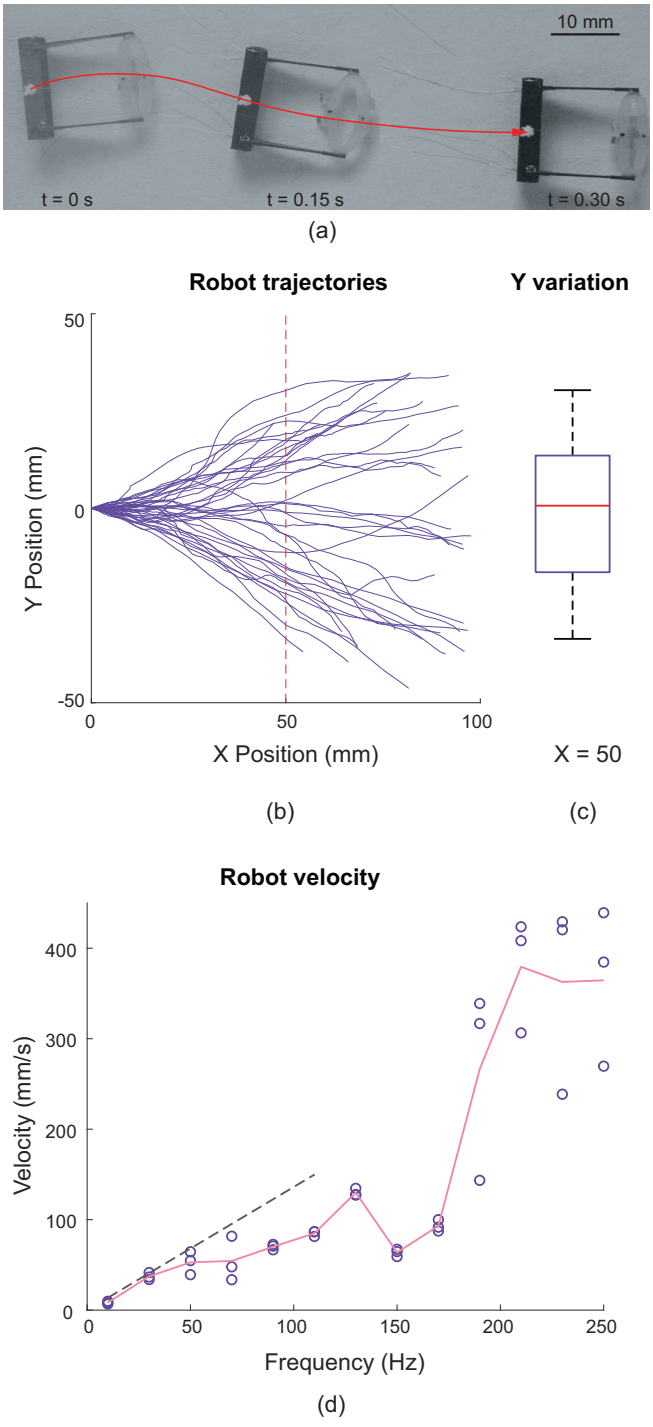

Fig. 5. Robot locomotion experiments. (a) Example of robot operating at 250 Hz. (b) Trajectories of robot open-loop operation. (c) Robot y variation at $x = 50$ mm. (d) Robot speed at different driving frequency. Circles are experiment trials. Red solid line is average velocity trend line. Gray dashed line is model trend line at low frequency.

of the robot, unpredicted ground reaction of the spines, drag of the wires, and other side effects. However, across 39 trials we recorded the lateral (y) deviation of the robot when it reached a forward distance of $x = 50$ mm. The mean value of the robot lateral variation is approximately 0, as shown in Fig. 5c, which suggests the robot has no steering preference

in open-loop. However, the wide range in lateral deviation does indicate the need for active feedback control of robot trajectory in future implementations.

Robot average velocities at different frequencies are shown in Fig. 5d. The sharp increase in speed that occurs as the frequency approaches 200 Hz matches closely the observed dynamic response of the soft transmission. This indicates that despite ground contact and sliding, the dynamic response of the robot appears consistent with that of the transmission-actuator combination. If the robot is not slipping, the speed should be proportional to the fore-aft amplitude of the transmission at the spines, multiplied by the stride frequency. The stride length, which can be also treated as the transmission output Δy, is relatively constant and low at lower driving frequency. Therefore, the increase of speed at low frequency is largely a result of the increase in driving frequency. We took the average of transmission output Δy from 10 Hz to 110 Hz as the robot stride length at lower frequency, and drew the predicted model trend line in Fig. 5d. The experiment data matches the model trend line pretty well. Robot velocity starts diverging from the trend line with the increase of frequency because slipping is more severe at higher frequency. The peak of the robot velocity at 130 Hz was caused by a secondary resonance mode of the soft transmission which can also be found in the frequency response. However, the robot reaches its maximum speed when it's operating around the dynamic resonance frequency of the transmission. Our recorded maximum average speed is 439 mm/s, equivalently 22 body lengths/s.

C. Travelling Wave in Soft Transmission

Robot turning behavior is a phenomenon that may utilize the soft behavior of the transmission. The soft transmission made from silicone rubber has the ability to generate complex shape change under different driving signals, which contributes to the turning of the robot. Using high-speed visualization and tracking we measured this shape change to observe the soft transmission shape change dynamics.

As shown is Fig. 6a, we describe the instantaneous shape of the transmission by the radius $\mathrm{R}(\theta)$ at given angle θ. $\mathrm{R}(\theta)$ is the radial distance from the center of the ellipsoid transmission to the contour of the transmission with an angle θ. When driving signals are applied on left and right sides of the transmission, the transmission will deform, causing shape change of the transmission contour. We tracked the axis length change $\Delta\mathrm{R}(\theta)$ of the transmission over time when it was driven by different signals. Heat maps were generated to depict the transmission contour shape change, with color reflecting the value of $\Delta\mathrm{R}(\theta)$. The x axis of the heat maps are θ ranging from $0 - 2\pi$; y axis is time over 3 driving cycles.

Piezoelectric actuation with simultaneous drive method [23] was used on the PZT actuators where tip displacement of an actuator is a linear map of the driving signal applied. When steering control was not engaged, i.e., two identical sinusoidal signals were applied to the PZT actuators, the transmission moved symmetrically along the central vertical axis (where $\theta = \pi/2$). Thus, $\Delta\mathrm{R}(\theta)$ was also symmetric all the time, Fig. 6b.

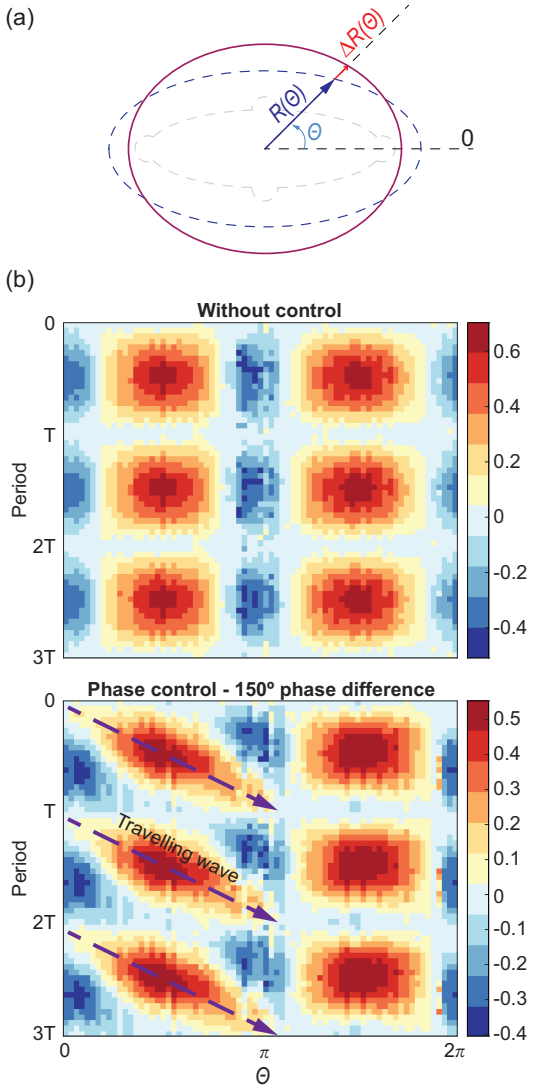

Fig. 6. Vibrational behavior of the soft transmission in straight and turning modes. a) Diagram of the deformation measurement. b) Space-time visualizations of transmission deformation with time on y-axis and angular position on x-axis. (Top) Without phase control the oscillations of the transmission are symmetric and periodic. (Bottom) With a phase difference between actuators we see the excitation of traveling waves that move from low to high θ.

When we changed the phase difference of the two sinusoidal signals, the shape change of the soft transmission became more complex. The right actuator was set to have a 150° phase lead ahead of the left one. A significant wave propagation was observed on the upper half rim of the transmission, while extra glue between the transmission and actuators at lower half rim likely limited the wave propagation motion. The wave motion is observed in Fig. 6b as the slope. This wave motion of the soft transmission is key to the robot steering in phase control.

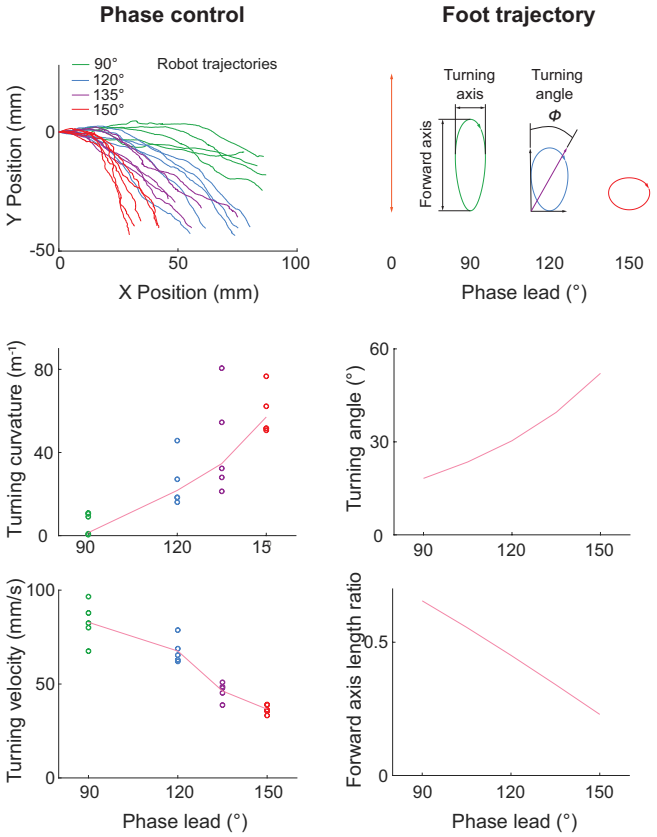

Fig. 7. Robot turning experiments. Left column: robot turning by phase control. Right column: robot foot trajectory predicted by kinematic model.

D. Robot Steering

The open-loop results indicate that the robot will tend to deviate from a straight path if left uncontrolled. Thus as a first step to implementing robot control we here investigate potential actuation methods that enable robot turning. From the observation of travelling waves in the soft transmission, we propose a robot steering strategy through phase control.

In phase control, we use phase differences between the left and right actuator to excite a traveling wave from left to right, or right to left. We achieved controlled turning by changing the phase difference of the two sinusoidal driving signals. The robot will turn left when the left actuator has phase lead over the right one, while it will turn right when the right actuator has phase lead over the left one. Since the turning control is symmetric, we tested only right turn behavior in this experiment. We each conducted 5 runs with varied phase difference from 90° to 150°. Robot trajectories are shown in Fig. 7(top, left), based on which we estimated the turning curvature (mid, left) and speed (bottom, left) for each run. The turning curvature increases with the phase lead while speed decrease with phase lead.

A simple flexure-linkage model of the transmission provided an estimate of the foot trajectories at different actuator phase lead/lag. When the phase difference is 0, the two actuators move symmetrically, driving the feet forward and backward on a straight line. When phase difference is introduced, feet trajectories become ellipse like, Fig. 7(top, right). We define the ellipse axis aligned with the robot body as the forward axis while the ellipse axis on the perpendicular direction as the turning axis. We also define the angle between the forward axis and the diagonal formed by the forward axis and the turning axis as the turning angle Φ.

The turning angle increases with the increasing phase difference between left and right actuator control signals. The turning angle likely contributes to the the turning ability of the robot. Comparison between robot turning curvature and the turning angle prediction in Fig. 7 shows good qualitative agreement between turning prediction and experiment. As the actuator phase difference increases from 0, the forward amplitude of the transmission motion decreases. We normalized the forward axis lengths at different phase difference to the maximum amplitude, at phase difference of 0. We find that the fore-aft displacement of the transmission decreases linearly as shown in Fig. 7(bottom, right). The decrease in amplitude reduces the effective stride length of the robot, and thus this is likely the cause of the lower the speed during turning.

IV. Conclusion

By combining smart-composite-manufacturing fabrication processes used for rigid robots, with a micro-machining and casting method employed for soft robotics, we have attempted to integrate soft robotic components into millimeter scale robots. Through dynamic characterization we identify that the soft transmissions achieve resonant behavior around 200 Hz oscillation frequencies. By driving these frequencies when the robot is in contact with the ground we were able to achieve remarkably high-speed ground locomotion for a millimeter scale robot; capable of moving at 439 mm/s which is equivalent to 22 body lengths/s, at resonance frequency. This work has focused on the design and control of the soft transmission system to enable rapid locomotion at resonant frequency and future work will explore integration of more soft robotic structures into the robot design ultimately aiming towards soft millimeter scale robots capable of high-speed movement.

V. Acknowledgment

We acknowledge funding support from the Mechanical & Aerospace Engineering Department. We thank Professor Michael Tolley for use of his micro-machining mill.

References

[1] J. J. Abbott, Z. Nagy, F. Beyeler, and B. J. Nelson, "Robotics in the small, part i: microbotics," *IEEE Robotics & Automation Magazine*, vol. 14, no. 2, pp. 92–103, 2007.

[2] S. Felton, M. Tolley, E. Demaine, D. Rus, and R. Wood, "A method for building self-folding machines," *Science*, vol. 345, no. 6197, pp. 644–646, 2014.

[3] J. M. Morrey, B. Lambrecht, A. D. Horchler, R. E. Ritzmann, and R. D. Quinn, "Highly mobile and robust small quadruped robots," in *Proceedings 2003 IEEE/RSJ International Conference on Intelligent Robots and Systems (IROS 2003)(Cat. No. 03CH37453)*, vol. 1. IEEE, 2003, pp. 82–87.

[4] A. M. Hoover, E. Steltz, and R. S. Fearing, "Roach: An autonomous 2.4 g crawling hexapod robot," in *2008 IEEE/RSJ International Conference on Intelligent Robots and Systems*. IEEE, 2008, pp. 26–33.

[5] A. T. Baisch, C. Heimlich, M. Karpelson, and R. J. Wood, "Hamr3: An autonomous 1.7 g ambulatory robot," in *2011 IEEE/RSJ International Conference on Intelligent Robots and Systems*. IEEE, 2011, pp. 5073–5079.

[6] M. Rogóż, H. Zeng, C. Xuan, D. S. Wiersma, and P. Wasylczyk, "Light-driven soft robot mimics caterpillar locomotion in natural scale," *Advanced Optical Materials*, vol. 4, no. 11, pp. 1689–1694, 2016.

[7] H. Lu, M. Zhang, Y. Yang, Q. Huang, T. Fukuda, Z. Wang, and Y. Shen, "A bioinspired multilegged soft millirobot that functions in both dry and wet conditions," *Nature communications*, vol. 9, no. 1, pp. 1–7, 2018.

[8] D. R. Frutiger, K. Vollmers, B. E. Kratochvil, and B. J. Nelson, "Small, fast, and under control: wireless resonant magnetic micro-agents," *The International Journal of Robotics Research*, vol. 29, no. 5, pp. 613–636, 2010.

[9] H.-W. Tung, M. Maffioli, D. R. Frutiger, K. M. Sivaraman, S. Pané, and B. J. Nelson, "Polymer-based wireless resonant magnetic microrobots," *IEEE Transactions on Robotics*, vol. 30, no. 1, pp. 26–32, 2013.

[10] R. St. Pierre, N. Paul, and S. Bergbreiter, "3dflex: A rapid prototyping approach for multi-material compliant mechanisms in millirobots," in *2017 IEEE International Conference on Robotics and Automation (ICRA)*. IEEE, 2017, pp. 3068–3073.

[11] R. St. Pierre, W. Gosrich, and S. Bergbreiter, "A 3d-printed 1 mg legged microrobot running at 15 body lengths per second," 2018.

[12] R. J. Wood, S. Avadhanula, R. Sahai, E. Steltz, and R. S. Fearing, "Microrobot design using fiber reinforced composites," *Journal of Mechanical Design*, vol. 130, no. 5, p. 052304, 2008.

[13] P. S. Sreetharan, J. P. Whitney, M. D. Strauss, and R. J. Wood, "Monolithic fabrication of millimeter-scale machines," *Journal of Micromechanics and Microengineering*, vol. 22, no. 5, p. 055027, 2012.

[14] R. J. Wood, "Design, fabrication, and analysis of a 3dof, 3cm flapping-wing mav," in *2007 IEEE/RSJ international conference on intelligent robots and systems*. IEEE, 2007, pp. 1576–1581.

[15] C. D. Onal, R. J. Wood, and D. Rus, "An origami-inspired approach to worm robots," *IEEE/ASME Transactions on Mechatronics*, vol. 18, no. 2, pp. 430–438, 2012.

[16] S. Miyashita, S. Guitron, M. Ludersdorfer, C. R. Sung, and D. Rus, "An untethered miniature origami robot that self-folds, walks, swims, and degrades," in *2015 IEEE International Conference on Robotics and Automation (ICRA)*. IEEE, 2015, pp. 1490–1496.

[17] W. Hu, G. Z. Lum, M. Mastrangeli, and M. Sitti, "Small-scale soft-bodied robot with multimodal locomotion," *Nature*, vol. 554, no. 7690, p. 81, 2018.

[18] E. Altshuler, J. M. Pastor, A. Garcimartín, I. Zuriguel, and D. Maza, "Vibrot, a simple device for the conversion of vibration into rotation mediated by friction: preliminary evaluation," *PloS one*, vol. 8, no. 8, 2013.

[19] F. Becker, S. Boerner, V. Lysenko, I. Zeidis, and K. Zimmermann, "On the mechanics of bristle-bots-modeling, simulation and experiments," in *ISR/Robotik 2014; 41st international symposium on robotics*. VDE, 2014, pp. 1–6.

[20] Y. Wu, J. K. Yim, J. Liang, Z. Shao, M. Qi, J. Zhong, Z. Luo, X. Yan, M. Zhang, X. Wang, *et al.*, "Insect-scale fast moving and ultrarobust soft robot," *Science Robotics*, vol. 4, no. 32, p. eaax1594, 2019.

[21] C. Laschi, B. Mazzolai, and M. Cianchetti, "Soft robotics: Technologies and systems pushing the boundaries of robot abilities," *Sci. Robot*, vol. 1, no. 1, p. eaah3690, 2016.

[22] R. Wood, E. Steltz, and R. Fearing, "Optimal energy density piezoelectric bending actuators," *Sensors and Actuators A: Physical*, vol. 119, no. 2, pp. 476–488, 2005.

[23] M. Karpelson, G.-Y. Wei, and R. J. Wood, "Driving high voltage piezoelectric actuators in microrobotic applications," *Sensors and actuators A: Physical*, vol. 176, pp. 78–89, 2012.

[24] N. Lobontiu and E. Garcia, "Analytical model of displacement amplification and stiffness optimization for a class of flexure-based compliant mechanisms," *Computers & structures*, vol. 81, no. 32, pp. 2797–2810, 2003.

[25] M. Ling, J. Cao, M. Zeng, J. Lin, and D. J. Inman, "Enhanced mathematical modeling of the displacement amplification ratio for piezoelectric compliant mechanisms," *Smart Materials and Structures*, vol. 25, no. 7, p. 075022, 2016.